Exergetic performance evaluation of louvered finned solar air heater: an experimental investigation

Subhash Chand[1], Harish Kumar Ghritlahre[2*] and Ajay Partap Singh[1]

*Correspondence:
harish.ghritlahre@gmail.com

[1] Department of Mechanical Engineering, IIMT University, Uttar Pradesh, Meerut 250001, India
[2] Department of Energy and Environmental Engineering, Chhattisgarh Swami Vivekanand Technical University, Bhilai, Chhattisgarh 491107, India

Abstract

Solar energy is a promising source of renewable energy, and solar air heaters are an important application for utilizing this energy source. This study investigates the exergetic performance of a louvered fin solar air heater (LFSAH) through experimental analysis conducted during day time from 9 am to 3 pm under identical operating and metrological parameters. Exergy analysis based on the 2nd law of thermodynamics is used to assess the quality of exergy losses and useful energy output and is deemed suitable for LFSAH design. The study experimentally examines the exergetic performance of LFSAH with various fin spacings and compares the results with those of a plane solar air heater (PSAH). The exergy efficiency is optimized by considering the fin spacing (ranging from 2 to 5 cm) and mass flow rate (MFR) (ranging from 0.007 to 0.0158 kg/s) through an exergy analysis of internal and exterior exergy losses. Based on the result analysis, the LFSAH's maximum exergy efficiency was achieved at 3.31% for a fin spacing of 2 cm and a MFR of 0.007 kg/s. The study found that incorporating louvered fins into the SAH substantially improves its exergetic performance compared to the PSAH.

Keywords: Exergy analysis, Fin spacing, Exergy efficiency, Louvered fins, Solar air heater

Introduction

The importance of energy in global economic progress and industrialization has grown significantly over time. However, due to the dwindling reserves of fossil fuels, there is an increasing focus on the development of non-conventional renewable energy sources. Among the many options available, geothermal, solar, biomass, wind, tidal, and hydro-electric power stand out [1, 2], with solar energy being one of the most popularly utilized sources of energy worldwide. Solar energy is a non-polluting, freely accessible fuel source. The most effective way to utilize solar energy is by converting it to thermal energy for use in SAH, as it ensures optimal utilization of this valuable resource.

Solar air heaters (SAHs) are the cheapest and most commonly used solar collectors due to their inherent simplicity. SAHs are primarily used for timber seasoning, industrial product curing, and space heating [3, 4], and they are also used in the field of building

Chand *et al. Journal of Engineering and Applied Science*   (2024) 71:145

Page 2 of 22

corruption side such as drying concrete, curing, and clay building components. SAHs play a vital role in solar heating systems due to their low material and cost requirements.

In a standard solar air heating system, the components include a collector frame with support structures, insulation, collector, and glass cover. The effectiveness of the system depends on several factors, including the design, tilted angle, material of collector, surface area, environmental conditions, MFR of the fluid heat transfer, and more, as detailed in references [5]. Therefore, achieving a cost-effective and efficient operation for many applications requires an optimal design of these components.

A solar collector, also known as the absorber plate, is the essential part of a SAH. It converts solar energy into thermal energy, which is then sent through a duct to the air that is moving. However, conventional SAHs function less well because of the absorber surface's low heat absorption capacity and the low thermal conductivity of the moving air. In order to address these issues, researchers have used various techniques, including extended surfaces [6–9], porous/packed beds [10–13], and artificial roughness [14–16], to increase the heat transfer coefficient and boost SAH's overall efficiency. Air-type collectors have a number of advantages, such as lower construction costs and overall weight as well as no worries about boiling, freezing, or pressure-related issues. To get around SAH's limitations, various kinds of theoretical models and experimental data have been used to verify the design parameters. Several factors, including depth, shape, collection length, number of glass covers, kind of absorber plate, and wind speed, affect the efficiency of SAH [17, 18]. In order to enhance the effectiveness of SAH, scientists have investigated various collector kinds, modified design parameters, and broadened their uses [19]. Though thermal analysis has been the primary approach used in earlier research to evaluate SAH performance [20], this approach overlooks internal losses. Thus, when assessing and contrasting solar thermal systems, exergy analysis—which measures the greater potential work feasible from energy—offers more thorough information and ought to be taken into account [21]. In order to maximize their effectiveness and achieve optimal exergy performance under certain operating and system settings, this study intends to investigate the thermal and exergy performance of various PSAHs in detail. According to Dincer and Rosen [22], exergy analysis is a strong thermodynamic approach that supports the development and analysis of thermal systems by fusing the principles of mass and energy conservation with the second law of thermodynamics. An effective technique for identifying and measuring inefficiencies in thermal systems is exergy analysis, which makes it possible to create designs that are more efficient. Exergy analysis identifies places where energy is wasted or lost by analyzing the movement of matter and energy inside a system. The system can then be optimized using this data, improving both its performance and energy efficiency. To put it briefly, exergy analysis is an essential tool for researchers and engineers who want to improve the efficiency and sustainability of thermal systems. A wide range of study has made use of the first and second laws of thermodynamics [23–29]. Kurtbas and Durmus [30] developed and evaluated five distinct SAC types based on their exergy and thermal efficiency. According to their findings, performance evaluations of SAH ought to focus on factors such as temperature differential (Tfo-Tfi), pressure loss, roughness geometry, and collector efficiency. Kurtbas and Turgut [31] conducted an investigation to examine the exergy and thermal analysis performance of SAH with both fixed and free fins. Their study's

Chand *et al. Journal of Engineering and Applied Science*   (2024) 71:145

Page 3 of 22

findings showed that the collector with free fins performed less well than the absorber plate with fixed fins. They also observed that exloss and heat transfer both show increases with an increase in pressure drop (ΔP). Karslı [17] evaluated the energetic and exergetic efficiency of a built Solar Air Collector used for drying applications. In order to do this, a system comprising four different types of absorber plate variations that have been experimentally examined was built. According to the findings, Collector Type A's thermal efficiency (ηI) varied from 26 to 80%, Type B's from 26 to 42%, Type C's from 60 to 70%, and Type D's from 26 to 64%. Moreover, it was shown that the exergetic efficiency (ηII) ranged from 0.27 to 0.64 for all collectors. Chand et al. [9] examined the thermal performance of LFSAH under the experimental investigation. The result reveals that the LFSAH performed better as compared with PSAH. Chand and Chand [32] analyzed the thermal performance of LFSAH at different louvered parameters. The results indicated that the thermal performance enhances from 43.14 to 76.79% with the use of louvered fines in solar collectors. Esen [33] performed an experiment on a DFSAH with absorber surfaces of two types: with and without obstacles. The author used flow rates of 0.015, 0.02, and 0.025 kg/s during the experiments. The results found by applying the concepts of energetic and exergetic efficiencies showed that the SAHs with obstacles outperformed the SAHs without obstacles under the similar operating conditions. Gupta and Kaushik [34] aimed to optimize the performance of a PSAH by investigating its exergy efficiency. They looked into the energetic performance of various factors such as MFR per unit collector area, aspect ratio, and duct depths. Their findings revealed that the maximum exergy output can be achieved when MFR is at its minimum and the inlet fluid temperature is low. Gupta and Kaushik [35] examined the effects of various roughness types on exergy, energy efficiency, and effective efficiencies. They looked at six different sorts of arrangements: metal mesh, wedge-shaped ribs, circular ribs, enlarged chamfered rib-groove, and V-shaped ribs. They developed a program with correlations to calculate ηI, ηII, and ηeff using MATLAB software. The results showed that adding roughness to the surface enhanced the efficiency when compared to a smooth one. Experiments were carried out by Akpinar and Kocyigit [19] to investigate the efficacy of a SAH fitted with barriers. They found that the thermal efficiency ranged from 20 to 82% using MFR of 0.0052 kg/s and 0.0074 kg/s. Exergetic performance, on the other hand, ranged from 8.32 to 44% in comparable operating conditions. The energy and energetic efficiency of a recently developed finned SAH and PSAH were studied by Alta et al. [20]. Using both single and double glass covers, they evaluated the collector's thermal and energy performance at different mass flow rates (MFR) and tilt angles (0 to 30°). They observed that the finned SAH with DGC outperformed the PSAH in terms of efficiency. The energy and exergetic performance of PBSAH integrating round capsules was investigated by Bouadila et al. [36]. The study participants observed that the daily energy efficiency (ηI) varied between 32 and 45%, and the daily energetic efficiency (ηII) varied between 13 and 25%. In an alternative study, Benli [37] conducted experimental investigations on the exergetic and energy efficiency of five distinct collector types, which included reverse trapeze and corrugated, corrugated trapeze, and flat plate collectors. Bayrak et al. [38] assessed the exergetic and energy efficiency of a collector plate with a porous baffled design. The experiments were carried out with MFR of 0.016 kg/s and 0.025 kg/s. They observed that the maximum values of ηth and ηII, along with

temperature difference, were attained with a porous material thickness of 6 mm at an MFR of 0.025 kg/s in case III. However, for case I, they observed the lowest values for the PSAH at MFR of 0.016 kg/s. Velmurugan and Kalaivanan [39] established an energy balance equation to assess the exergy and energy analysis of single, double, and triple pass SAH. They used MATLAB software to program a simulation code for calculating the thermal and exergy efficiency, and studied the effect of MFR on exergetic performance, energetic performance, improvement potential, temperature rise, and irreversibility. They concluded that the triple pass solar collector performs better compared with double pass and PSAH. Acır et al. [40] investigated the exergy and energy performance of a novel SAC with circular turbulator collectors. They conducted studies with four copper tubes painted black and having varied obstacle relief angles (45°, 90°, and 135) with MFR range from 0.0023 to 0.0055 kg/s. According to their findings, the ηII varied from 8.1 to 42.4% and the ηI ranged from 28.6 to 79.5%. For MFR 0.0055 kg/s with a 45° obstacle relief angle, the highest ηI and ηII values were recorded. Ghritlahre and Prasad [41] implemented a neural model to estimate the energetic and exergetic performance of SAH with roughened surfaces. They performed experiments with roughness solar collector with various MFR range from 0.010 to 0.0175 kg/s to calculate the ηI and ηII. They analyzed a neural model with study of 2 output and 6 input variables and usage of 60 sets data of experimental in neural model. The optimal neural model for prediction was found to be the 6–6-2 neural model trained using the Levenberg–Marquardt (LM) training algorithm. Abuşka [42] experimentally analyzed the exergetic and energetic performance of conical surface SAH with various MFR range from 0.04 to 0.01 kg/s. The result indicated that the thermal and exergy efficiency were obtained at 63.2–57.2%, 71.5–61.7%, 74.6–64.0%, and 19.3–16.1%, 15.1–11.5%, 12.5–9.2% for MFR of 0.04 kg/s, 0.08 kg/s, and 0.10 kg/s respectively for conical and PSAH. They also observed that the thermal performance was enhanced by 10% compared to PSAH. Matheswaran et al. [43] conducted an analytical investigation of ηI and ηII for a SAC with a double duct jet surface with single pass. They developed a MATLAB program to calculate exergy and energy efficiency, and also they developed a correlations for using various factor like jet plate design parameters and Reynolds number. Aktaş et al. [44, 45] established a designed a multi-pass solar collector (MPSAC) with perforated fins and investigated its thermal and exergetic performances through experiments conducted under the MFR of 0.0069 kg/s and 0.0087 kg/s. The results revealed that the thermal efficiency of DPSAC and MPSAC were varied from 30.37 to 69.03% and 48.88 to 83.47%, respectively. Furthermore they observed that the exergy performance of DPSAC and MPSAC varied from 2.10 to 17.12% and 8.74 to 23.97%, respectively. According to the literature study, it was observed that the second law analysis of the SAH provides a clear understanding of the efficient utilization of solar energy to heat the air. It is also observed that no research has been performed on the exergetic performance analysis of LFSAH. Therefore, the present study aims to examine the exergetic performance analysis of LFSAH. Kumar and Layak [46] investigated the analytical approach to enhance the energy and exergy performance of a twisted-rib roughness absorber collector. They observed that the enhancement in thermal efficiency (ηth), exergy efficiency (ηexergy), and overall efficiency (ηeff) were 1.81, 1.81, and 1.79 times higher, respectively, compared to PSAH. Amit and Layak [47] designed a novel winglet-type roughness SAH and conducted experiments to

Chand *et al. Journal of Engineering and Applied Science*   (2024) 71:145

Page 5 of 22

analyze its performance using thermal, effective, and exergetic analysis concepts. The analysis results indicated a notable improvement in performance for the SAH with a winglet-type roughness absorber surface in comparison to a smooth plate absorber. Specifically, the optimum values for thermal, effective, and exergetic efficiencies were found to be 2.12, 1.99, and 2.03 times higher than PSAH. Kumar et al. [48] conducted a SAH that incorporated copper tubes with a zig-zag design. When tested under comparable weather circumstances, they discovered that the SAH with copper tubes had greater thermal and energy efficiency than one without. In natural convection conditions, the energy efficiency of the SAH with copper tubes fluctuated between 14.53 and 20.36%, with an average of 18.26%. In contrast, the absorber without copper tubes exhibited efficiency ranging from 12.45 to 17.53%, with an average of 16.29%. The exergetic efficiency for both types of SAH ranged between 0.95 and 1.939% and 1.2 and 1.53%, with an average of 1.41% and 1.69%, respectively. Das [49] conducted an experiment to examine the performance of a stationary SAH versus a movable one. The movable SAH proved to be superior in several aspects based on two assessment methods. Notably, the movable SAH displayed double the average heat transfer value, 47.8% thermal efficiency, 2.4 times exergetic efficiency, 20% higher performance coefficient, and 23.8% higher average collector outlet temperature than the stationary SAH. Prakash et al. [50] studied the performance of a hybrid mode double-pass solar air heater (DPSAH) using exergy and thermal analysis. According to their findings, the average exergy and energy efficiency for natural convection mode were 2% and 11.47%, respectively. For the induced forced convection mode, the exergetic and energetic performance were 10.43% and 56%, respectively. However, the addition of a reflector increased the exergy and energy efficiency to 17.617% and 86.19%, respectively. In their study, Khanlari et al. [51] investigated a vertical SAH that utilized a perforated baffle plate and an absorber coated with nanoparticles. Using both analytical and experimental techniques, they evaluated the heaters' performance and found that the heaters with nanoparticles had a thermal efficiency range of 58.10 to 76.22% and the heaters without nanoparticles had a range of 54.96 to 72.05%. Moreover, they observed that the application of a nanoparticle-embedded coating raised exergy efficiency by 9.25 to 10.58%.

From the literature review, it is evident that numerous studies have been conducted by various researchers to assess the exergetic performance of different types of SAH, including roughened, extended surface, packed/porous bed, and finned absorber SAHs. However, there is a notable lack of research on finned absorbers, particularly those with louvered fins. For LFSAH, only theoretical investigations have been conducted thus far, with no experimental studies on louvered fins SAHs being conducted yet. This study was undertaken to analyze the performance of a SAH equipped with louvered fins, considering outdoor conditions and conducting exergy analysis.

The current investigation is centered on the design of a novel LFSAH absorber plate, with a focus on assessing its exergetic performance through experiments conducted in Jamshedpur, India. The study seeks to accomplish the following objectives: Conduct experiments with different MFR using a louvered fin absorber plate.

 (i)   Evaluate the performances based on second law efficiency.
(ii)   Analyze the SAH performances with different parameters of fin space and MFR.
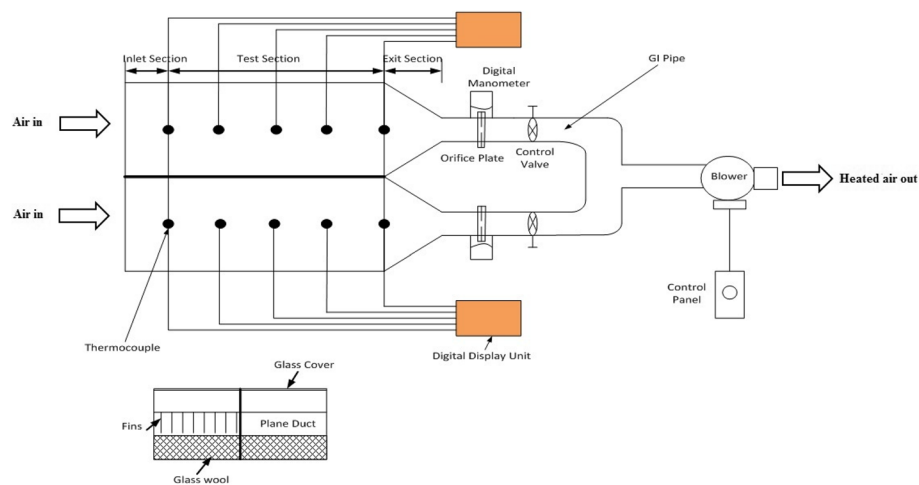(iii) Evaluate the potential for exergy destruction and improvement at various parameters.

Chand *et al. Journal of Engineering and Applied Science*   (2024) 71:145

Page 6 of 22

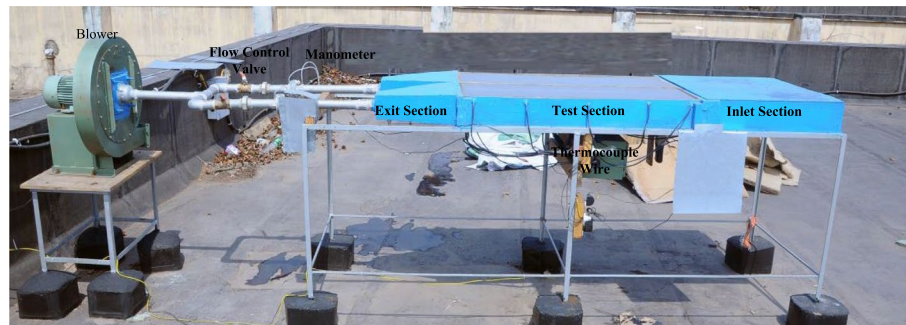**Fig. 1** Diagram of the experimental arrangement

Fig. 2 Pictorial view of experimental arrangement

This objective aims to evaluate the magnitude of exergy destruction within the system and identify potential enhancements to improve the system's performance. In summary, the primary goal of this study is to offer insights into the performance of a SAH featuring a louvered fin collector plate and to identify potential avenues for optimizing the system's efficiency.

Methods

Experimental setup description

Figure 1 illustrates the schematic representation of a single-pass SAH. In this setup, both the louvered finned and smooth collectors were situated 5 cm above the base. Throughout the experiment, the air circulation through the collectors followed the converging segment, leading into the orifice meter for the measurement of airflow rate. Figure 2 presents the picture of both the finned and flat SAH. The collector's outlet was linked to the wooden convergent section using GI pipes, an orifice meter, a flow control valve, and a 3-hp blower. Various flow rates were achieved by adjusting the flow control valve.

Twenty-four thermocouples were fitted in order to measure the intake temperature (T_{in}), plate temperature (T_p), and exit temperature (T_{out}). To be more precise, each absorber plate's temperature was monitored by five thermocouples (Fig. 3), and the air temperature inside the ducts was monitored by seven thermocouples that were positioned in a strategic
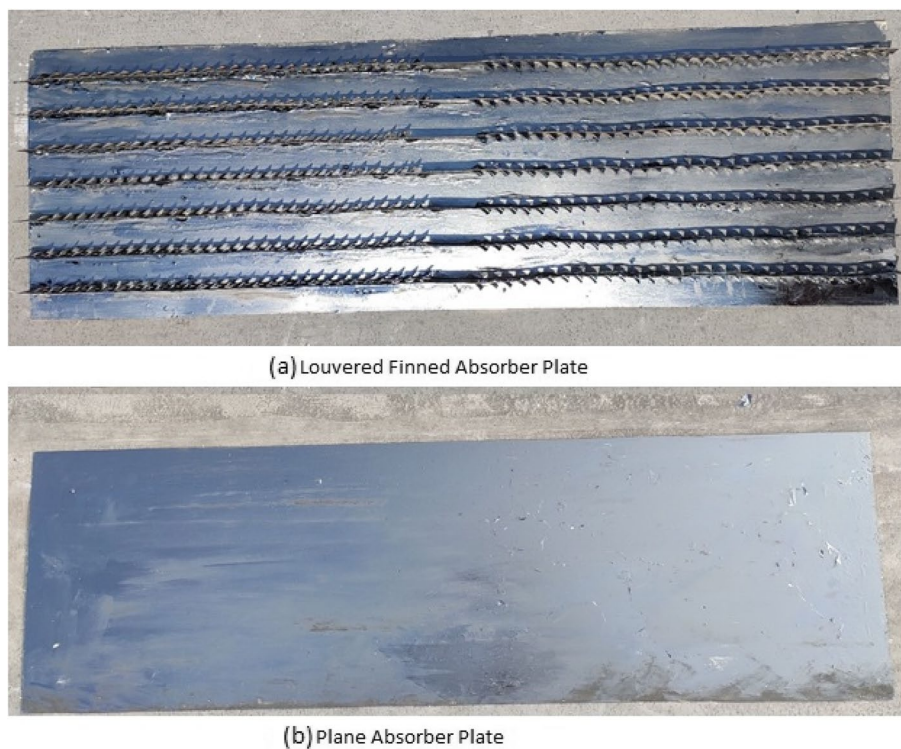
(a) Louvered Finned Absorber Plate

(b) Plane Absorber Plate

Fig. 3 Absorber plates

manner. The locating of thermocouples across the test section for monitoring air and plate temperatures is depicted in Fig. 4. Furthermore, a pyranometer, as depicted in Fig. 5, was employed to gauge insolation levels throughout the experiment. The outdoor experiments were conducted from 9 am to 3 pm in January and February of 2018 on clear-sky days. A flow control valve was utilized in order to regulate the MFR inside the duct. Both channels were permitted to circulate air for a minimum of 120 min before data recording commenced. Subsequently, the flow was maintained at a constant rate, and data collection was initiated. Measurements of manometer, inlet temperature, wind speed, outlet temperature, and insolation were recorded at 30-min intervals, spanning from 9:00 am to 3:00 pm.

The airflow measurement in the duct is achieved using an orifice meter connected to a digital manometer, which is installed in line with the mild steel pipe. The orifice meter was calibrated by installing it in series with a calibrated orifice plate of known coefficient of discharge. The MFR of air was calculated based on the observed pressure drop in centimeters of water (cm H_2O). The investigation's MFR has been documented in Table 1.

The pressure drop across the test length was measured using a digital micro manometer. J-type thermocouples coupled to a digital data recorder were used to monitor the temperature of the absorber plate, the exit and inlet air, and both. The data loggers from Countron have an accuracy of ± 1 °C. The thermocouples were calibrated under similar environmental conditions. A calibration test demonstrated that the thermocouple readings were accurate to within ± 1 °C.

The positions of the thermocouples for measuring air and plate temperatures over the test section are illustrated in Fig. 4. The pyranometer was also used to measure sun radiation.
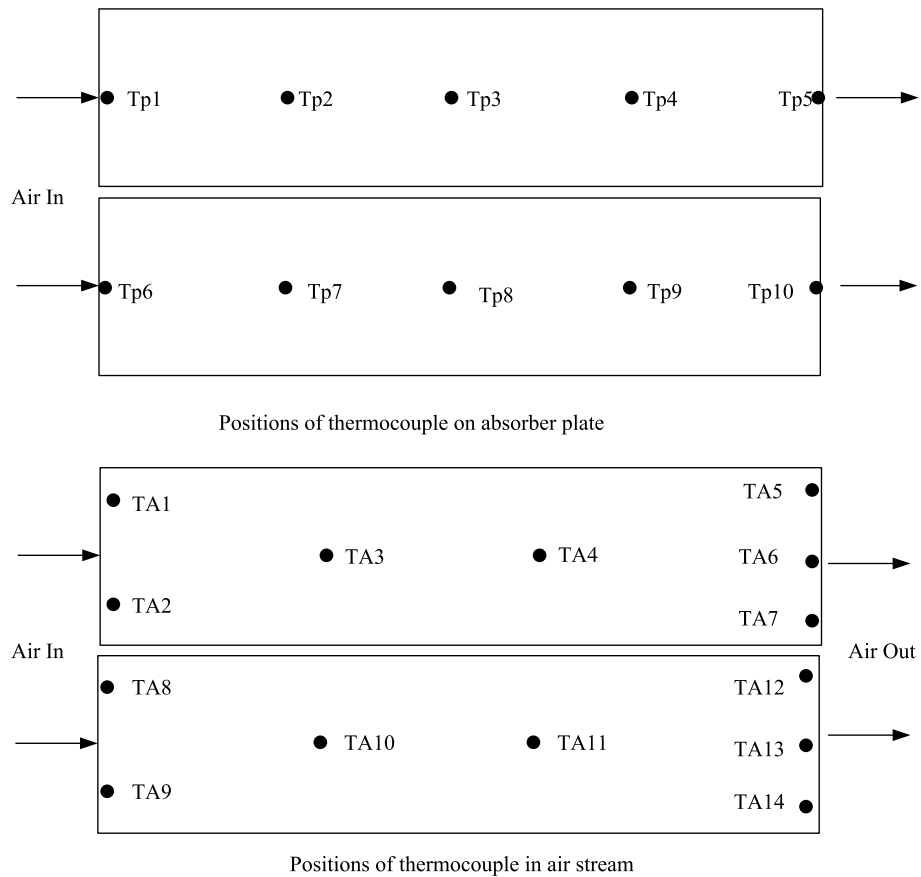
Chand *et al. Journal of Engineering and Applied Science* (2024) 71:145

Page 8 of 22

Positions of thermocouple on absorber plate

Positions of thermocouple in air stream

Fig. 4 Thermocouple position in absorber and duct

Fig. 5 Pyranometer with digital display unit

Uncertainty analysis

A method for analyzing design and experimental measurement error is uncertainty analysis. Moreover, the error analysis shows a correlation between the error interval and the recorded experimental results. Kline and Mc Clintock [52] presented the uncertainty analysis. The

Table 1 Measurement of MFR of air

Sl. No	ΔP (cm H$_2$O)	$\dot{m}$(kg/hr)	$\dot{m}$(kg/s)
1	5	25.37	0.0070
2	10	35.88	0.009
3	15	43.94	0.012
4	20	50.74	0.014
5	25	56.73	0.0158

Table 2 Uncertainty analysis of different parameters

Sl. No	Measuring devices	Uncertainty
1	Insolation	±1
2	Orifice plate	±0.1
3	Duct pressure drop	±0.1 mbar
4	Temperature measurement unit	±1°C
5	Duct width: W and length: L	±1
6	Pressure drop at orifice	±0.1 cm H$_2$O
7	Duct height, H	±0.1

experimental error measurement is shown in Table 2. The error in measurement of "ψ" may be stated as follows if the uncertainty of any criterion is determined using specific quantities:

$$\frac{\delta\psi}{\psi} = \left[\left(\frac{\delta\psi}{\partial y_1}\delta y_1\right)^2 + \left(\frac{\delta\psi}{\partial y_2}\delta y_2\right)^2 + \ldots\ldots\ldots + \left(\frac{\delta\psi}{\partial y_n}\delta y_n\right)^2\right]^{1/2} \tag{1}$$

where $\delta\psi$ and $y_1, y_2\ldots\ldots y_n$. $\frac{\delta\psi}{\psi}$ and $\delta y_1, \delta y_2\ldots\ldots\delta y_n$. The measurement errors are recognized as absolute uncertainty and relative uncertainty, respectively.

Flow rate ($\dot{m}$)

$$\dot{m} = C_d A_o \left[\frac{2\rho\Delta P}{1-\beta^4}\right]^{0.5} \tag{2}$$

$$\frac{\delta\dot{m}}{\dot{m}} = \left[\left(\frac{\delta C_d}{C_d}\right)^2 + \left(\frac{\delta A_o}{A_o}\right)^2 + \frac{1}{4}\left(\frac{\delta\Delta P}{\Delta P}\right)^2 + \frac{1}{4}\left(\frac{\delta\rho}{\rho}\right)^2 + \frac{1}{4}\left(\frac{\delta\beta}{\beta}\right)^2\right]^{1/2} \tag{3}$$

Thermal efficiency (η)

$$\eta = \frac{\dot{m}\,C_p(T_o - T_i)}{I \times A_c} \tag{4}$$

Equation (1) shows the uncertainty analysis of efficiency calculation as a function of $\dot{m}$, ΔT, and I where A_c and C_p are taken as constants.

$$\frac{\delta\eta}{\eta} = \left[\left(\frac{\delta\dot{m}}{\dot{m}}\right)^2 + \left(\frac{\delta\Delta T}{\Delta T}\right)^2 + \left(\frac{\delta I}{I}\right)^2\right]^{1/2} \tag{5}$$

The uncertainty of η and $\dot{m}$ are 0.0290 and 0.0278, respectively.

Exergetic performance analysis

The optimal utilization of energy can be achieved through the analysis of a system's exergy, which is a highly useful concept. Such an analysis can facilitate the efficient operation and design of thermal systems. The 2nd law efficiency of a system is determined by the ratio of exergy gained to exergy input. It should be noted that the current analysis is subject to the following assumptions:

1. It is assumed that the system is in a state of steady-state.
2. The effects of potential energy (PE) and kinetic energy (KE) can be disregarded.
3. The system is assumed to be homogenous.
4. Air-specific heat always remain constant so we can consider it as ideal fluid.
5. The system experiences positive work transfer and heat transfer.

In general, the energy and exergy balance equations (Fig. 6), which usually neglect potential and kinetic energies, can be formulated in the form of rate equations [53–55]:

$$\sum \dot{E}_i = \sum \dot{E}_o \tag{6}$$

$$\left(\sum \dot{Ex}_i - \sum \dot{Ex}_o \right) = \sum \dot{Ex}_{Loss} \tag{7}$$

where

$$\sum \dot{Ex}_{Loss} = \left(\sum_{Loss(external)} \dot{Ex} + \sum_{Dest(internal)} \dot{Ex} \right) \tag{8}$$

$$\sum_{Dest} \dot{Ex} = \sum_{Heat} \dot{Ex} - \sum_{Work} \dot{Ex} + \sum_{Mass,in} \dot{Ex} - \sum_{Mass,out} \dot{Ex} - \sum_{Loss(external)} \dot{Ex} \tag{9}$$

The Eq. (9) can also be simplified as:
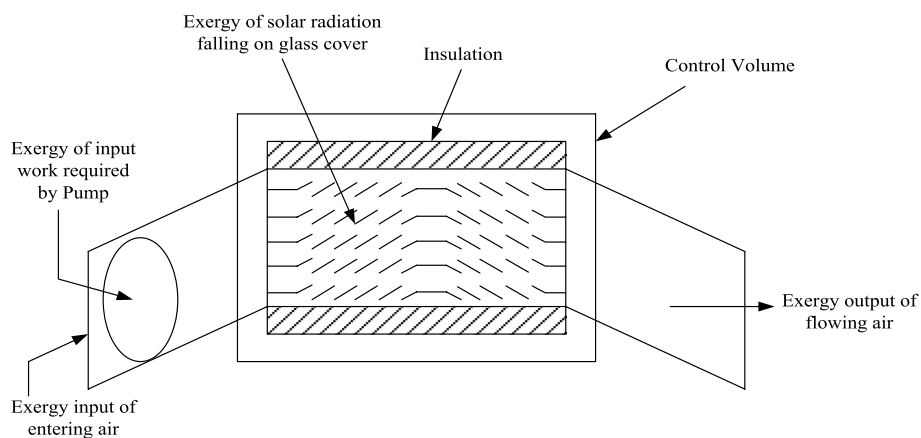
Fig. 6 Exergy flow diagram for a solar air heater with louvered fins

Chand *et al. Journal of Engineering and Applied Science*   (2024) 71:145

Page 11 of 22

$$\sum_{Dest} \dot{Ex} = \sum_{Heat} \dot{Ex} - \dot{W} + \sum \dot{m}_i \, \psi_i - \sum \dot{m}_o \, \psi_o - \sum_{Loss(external)} \dot{Ex} \tag{10}$$

From the Petela equation, exergy of insolation falling on glass cover, $\sum Ex_{Heat}$ can be given as [56]:

$$\sum Ex_i = \sum Ex_{Heat} = IA_c \left[1 - \frac{4}{3} \left(\frac{T_{amb}}{T_{sun}} \right) + \frac{1}{3} \left(\frac{T_{amb}}{T_{sun}} \right)^4 \right] \tag{11}$$

Therefore, at the inlet and outlet, the specific exergy can be expressed as:

$$\Psi_o = (h_o - h_e) - T_a (S_o - S_e) \tag{12}$$

$$\Psi_i = (h_i - h_e) - T_a (S_i - S_e) \tag{13}$$

In Eq. (10), the external loss is calculated by the following equation [54]:

$$\sum_{Loss(external)} \dot{Ex} = \sum_{Loss(optical)} \dot{Ex} = (1 - \tau \alpha) IA_c \left[1 - \frac{4}{3} \left(\frac{T_{amb}}{T_{sun}} \right) + \frac{1}{3} \left(\frac{T_{amb}}{T_{sun}} \right)^4 \right] \tag{14}$$

From Eqs. (11), (12), (13), and (14), put in Eq. (10) and the resulting equation becomes:

$$\left[1 - \frac{4}{3} \left(\frac{T_{amb}}{T_{sun}} \right) + \frac{1}{3} \left(\frac{T_{amb}}{T_{sun}} \right)^4 \right] \dot{Q}_c - \dot{m} \left[(h_o - h_i) - T_a (s_o - s_i) \right] - (1 - \tau \alpha) IA_c \left[1 - \frac{4}{3} \left(\frac{T_{amb}}{T_{sun}} \right) + \frac{1}{3} \left(\frac{T_{amb}}{T_{sun}} \right)^4 \right] = \sum_{Dest} \dot{Ex} \tag{15}$$

where

$$\dot{Q}_c = IA_C \text{ and } \dot{W} = 0 \tag{16}$$

The variations in the entropy and enthalpy of the air can be written as:

$$\Delta s_{air} = s_o - s_i = C_{pf} ln \frac{T_{fo}}{T_{fi}} - R ln \frac{P_o}{P_i} \tag{17}$$

$$\Delta h_{air} = h_o - h_i = C_{pf} \left(T_{fo} - T_{fi} \right) \tag{18}$$

The following expression is obtained by putting the Eqs. (16), (17), and (18) in Eq. (15).

$$\left[1 - \frac{4}{3} \left(\frac{T_{amb}}{T_{sun}} \right) + \frac{1}{3} \left(\frac{T_{amb}}{T_{sun}} \right) \right] IA_c - m C_{pf} (T_{fo} - T_{fi}) + m T_a \left(C_{pf} \, mathrm{ln} \frac{T_{fo}}{T_{fi}} - R ln \frac{P_o}{P_i} \right) - (1 - \tau \alpha) IA_c \left[1 - \frac{4}{3} \left(\frac{T_{amb}}{T_{sun}} \right) + \frac{1}{3} \left(\frac{T_{amb}}{T_{sun}} \right)^4 \right] = \sum Ex_{dest} \tag{19}$$

The exergetic efficiency of SAH [51]:

$$\eta_{2nd} = \left(\frac{\sum_o \dot{Ex}}{\sum_i \dot{Ex}} \right) = \left(1 - \frac{\sum_{Loss} \dot{Ex}}{\sum_i \dot{Ex}} \right) \tag{20}$$

In the context of exergetic analysis of different processes or systems, Van Gool [57] proposed the concept of "Improvement Potential," which is expressed as follows:

$$\dot{IP} = (1 - \eta_{2nd}) \, \dot{Ex}_{Dest} \tag{21}$$

Results and discussion

Experimental research on the effects of LFSAH at various fin spacings has been conducted in Jamshedpur, India, during the winter months of January and February 2018. Jamshedpur, an Indian city, is situated at the geographical coordinates of 22.77° N and 86.14° E. The experiment involved testing different louvered fin spacings, with MFR from (0.007 to 0.0158) kg/s. Table 3 presents the design and operating parameters that were taken into account for the analysis.

Figure 7 illustrates how insolation changes throughout the day for varying fin spacing ranging from 2 to 5 cm, and the range of MFR 0.007 to 0.015 8 kg/s, at which the experiment is performed. In solar collectors, the quantity of instantaneous radiation serves as a crucial parameter. The intensity of solar radiation begins to rise at dawn and reaches its peak at noon, followed by a gradual decline. In February, the peak insolation value is 866.37 W/m^2 at 12:30 pm. Compared to February, January exhibited the lowest ambient temperature. Furthermore, the average solar intensity for experiments conducted on louvered fins with pitch of 2 to 5 cm were 650.03, 600.62, 565.66, and 589.06 W/m^2, respectively.

Figure 8 displays the correlation between exergy efficacy and various time periods, and different MFR (0.007–0.0158) kg/s, and fin spacings ranging from 2 to 5 cm for both LFSAH and PSAH. The outcomes indicate that the highest exergy efficiency is achieved between 12:00 to 1:00 h, following which it gradually decreases. It has been observed that LFSAH outperforms PSAH in terms of exergy efficiency across all fin spacings. Exergy efficiencies of 3.31%, 2.3%, and 0.93% were achieved for fin spacings of 2 cm, 5 cm, and PSAH, respectively, at an MFR of 0.007 kg/s. Moreover, there were observed exergy efficiency variations of around 2.5 and 1.47 times compared to PSAH for fin spacings of 2 cm and 5 cm, respectively.

In Fig. 9, the exergetic performance pattern for all experiments conducted that day is displayed for PSAH, 2 cm and 5 cm fin spacings. The results indicate that as the MFR increased from 0.007 to 0.0158 kg/s, the exergetic performance of all collector types decreased. Additionally, compared to the PSAH and LFSAH with a spacing of 5 cm, 2 cm displayed superior exergy efficiency.

Table 3 System and operating parameters

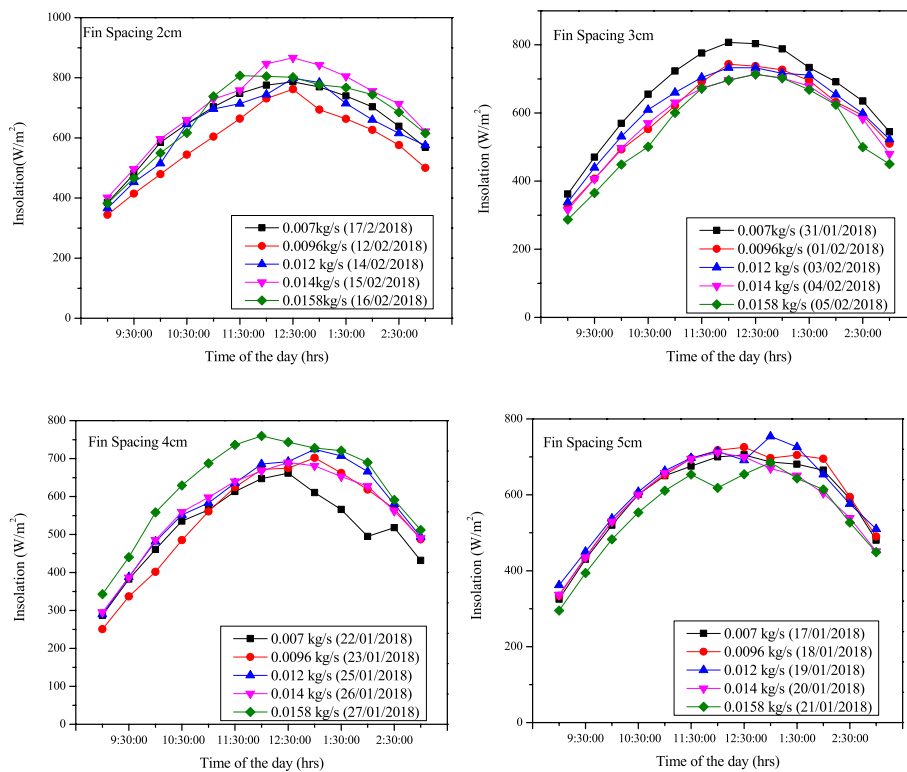| Parameters	Value	Parameters	Value
Width of absorber plate	400 cm	Louvered pitch, length, and angle	2.5 cm, 2.5 cm, 20°
Length of absorber plate	120 cm	Fin spacing	2, 3, 4, 5 cm
Duct height	5 cm	Flow rate	0.007–0.0158 kg/s
Fin height	3.5 cm		
Insulation thickness	5 cm		
Fin thickness	0.1 cm		

Fig. 7 Variation of solar Intensity with standard daytime for fins pitch of **a** 2 cm, **b** 3 cm, **c** 4 cm, and **d** 5 cm at different MFR from 0.007 to 0.0158 kg/s

The comparison between the exergy efficiency of louvered fins with varying spacing and PSAH at different MFR is presented in Fig. 10. The graph highlights that the exergy efficiency decreases with increasing MFR. A fin spacing of 2 cm exhibits a significantly higher exergy efficiency of 3.3% compared to 2.3% and 0.93% for fin spacings of 5 cm and PSAH, respectively. This trend remains consistent even at a lower MFR of 0.007 kg/s. The cause of this effect is the absorption of insolation by the collector, resulting in higher exergy loss and lower exergy efficiency values, regardless of the MFR values. This trend is particularly evident at higher MFR, where the high pump work required outweighs the exergy of heat energy collected.

Figure 11 shows that the exergy destruction of louvered fins pitch at 2 to 5 cm and PSAH at varying MFR. This result leads to the increasing nature of the exergy destruction with MFR. This behavior is similar to compared with PSAH. The reason for this is that at higher values of MFR, the exergy losses due to friction and pressure also increase, resulting in the exergy input not being able to overcome these losses. To increase the amount of useful work that can be obtained from the system and reduce exergy destruction, the performance of the collector can be improved.

Figure 12 shows that the improvement potential of louvered fins pitch at 2 to 5 cm and PSAH at varying MFR. This result leads to the increasing nature of the improvement potential with MFR. This behavior is similar to compared with PSAH. From Fig. 12, it can be observed that as the MFR increases, the system needs to have more improvement potential.
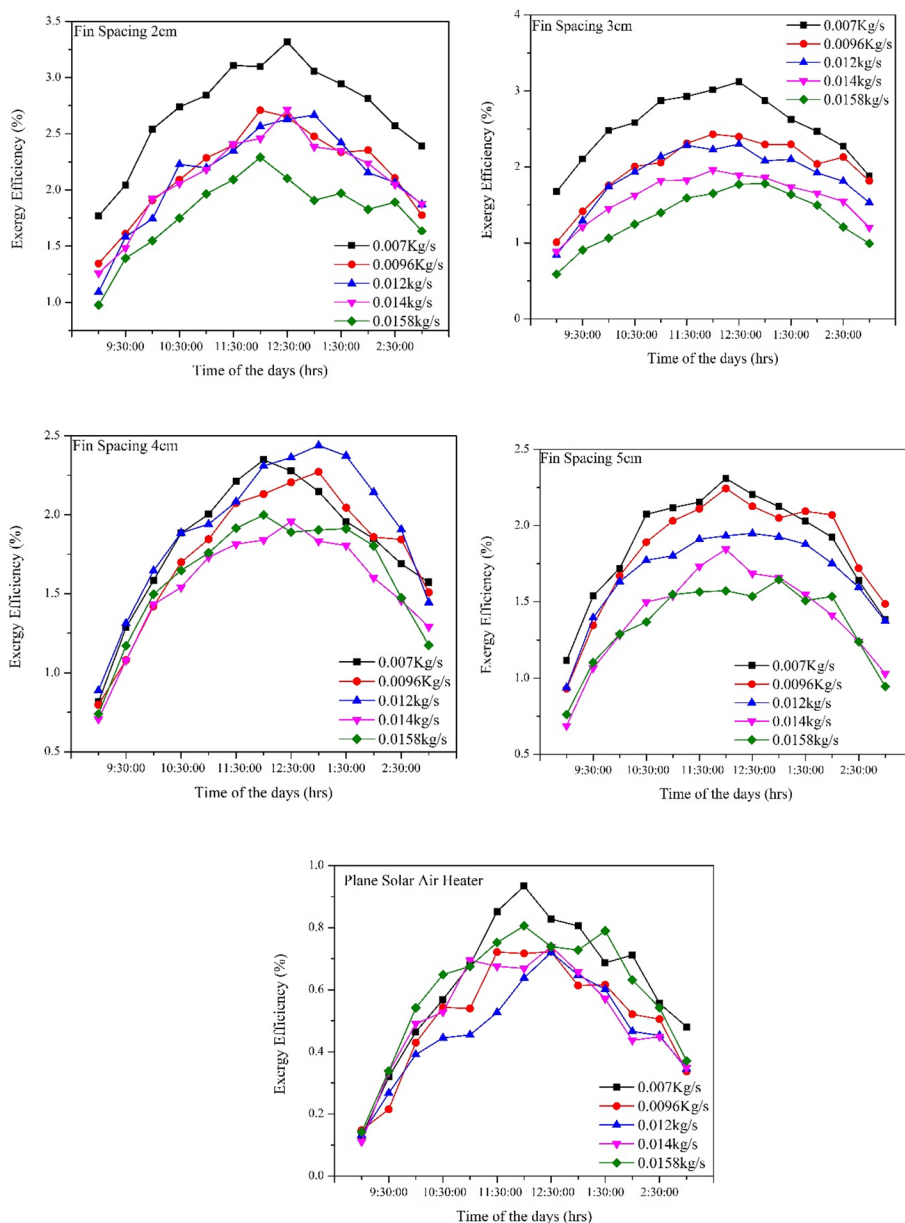
Chand *et al. Journal of Engineering and Applied Science*   (2024) 71:145

Page 14 of 22

Fig. 8 Variation in exergy efficiency at different MFR for various fin spacings, namely **a** 2 cm, **b** 3 cm, **c** 4 cm, **d** 5 cm, and **e** PSAH

To ensure the precision of the outcomes, it is necessary to validate the results, a comparison was conducted between the exergy efficiency of the present PSAH and the LFSAH proposed by Sabzpooshani et al. [58]. Figure 13 illustrates this comparison, with the mean deviations of exergy efficiency between the two systems calculated to be 13.8%. The results revealed that, for an MFR ranging from 0.007 to 0.0158 kg/s, the average enhancement in exergy efficiency for the LFSAH was 3.7 times higher than that of the PSAH. These findings suggest that the current experimental work is consistent with the findings of Sabzpooshani et al. [58], which provides greater confidence in the extension of the present research of louvered fin discussed in this research.
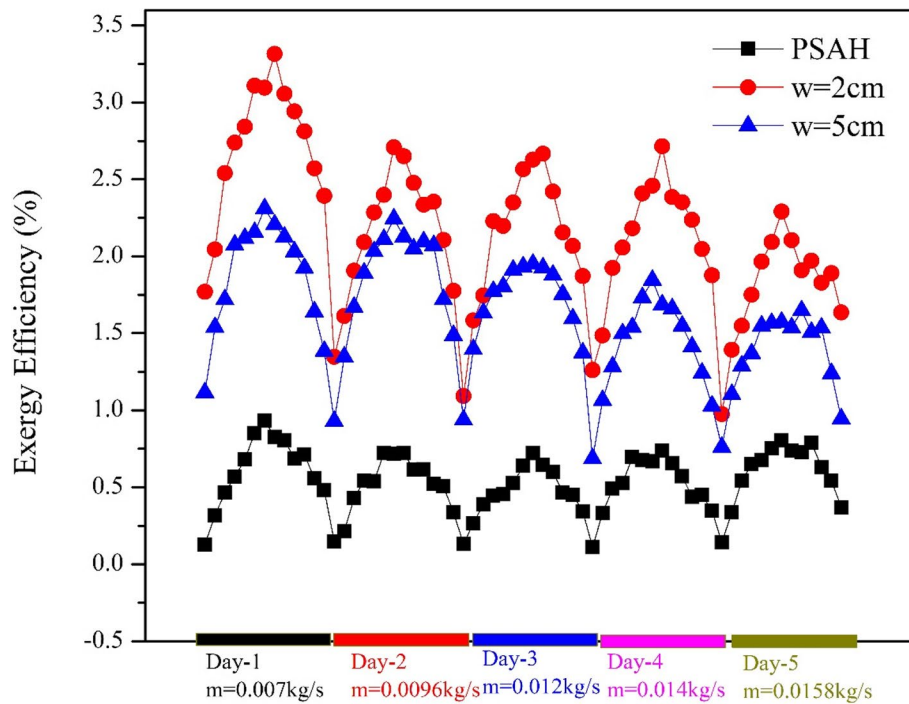
Fig. 9 The variation on exergy efficiency for entire days of experiments at fin spacing 2 cm, 5 cm, and PSAH
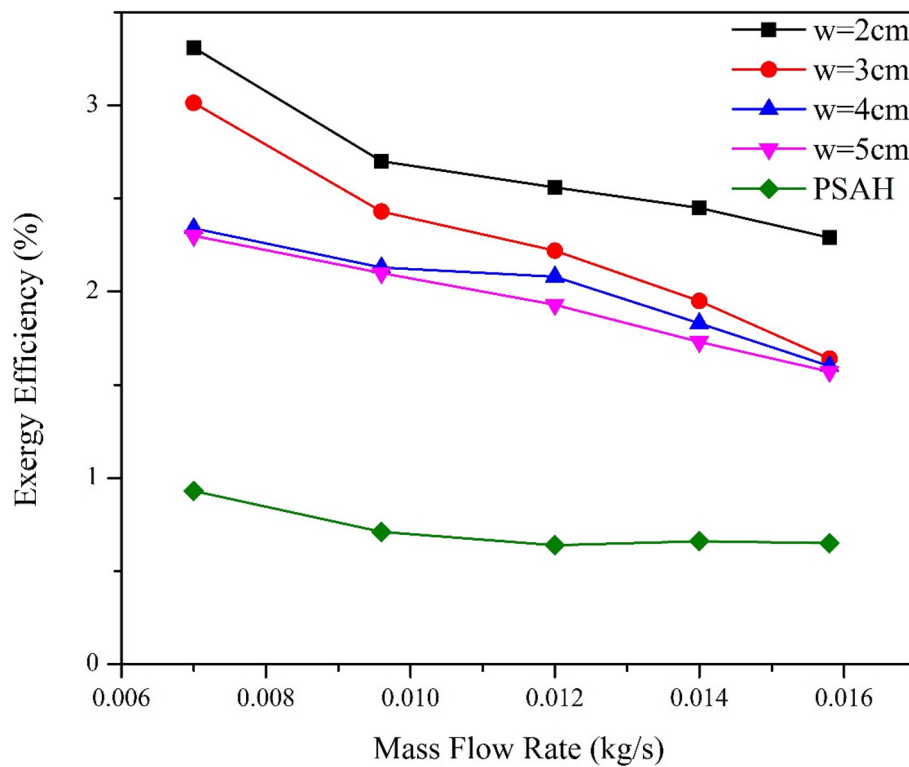

Fig. 10 Demonstrates the relationship between exergy efficiency and MFR for various louvered fin spacings
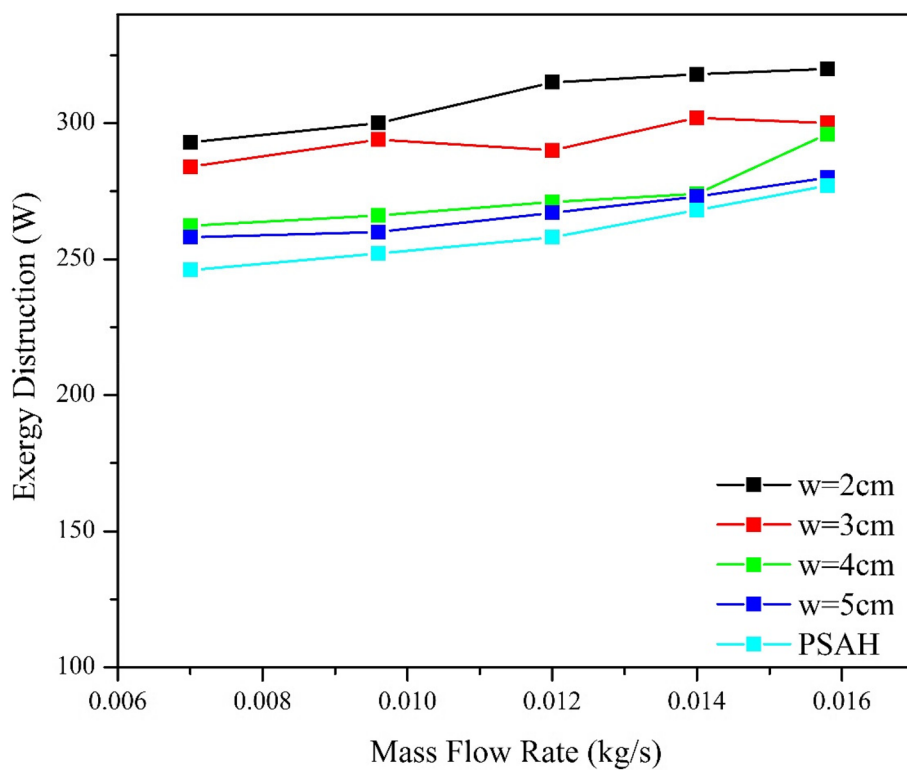
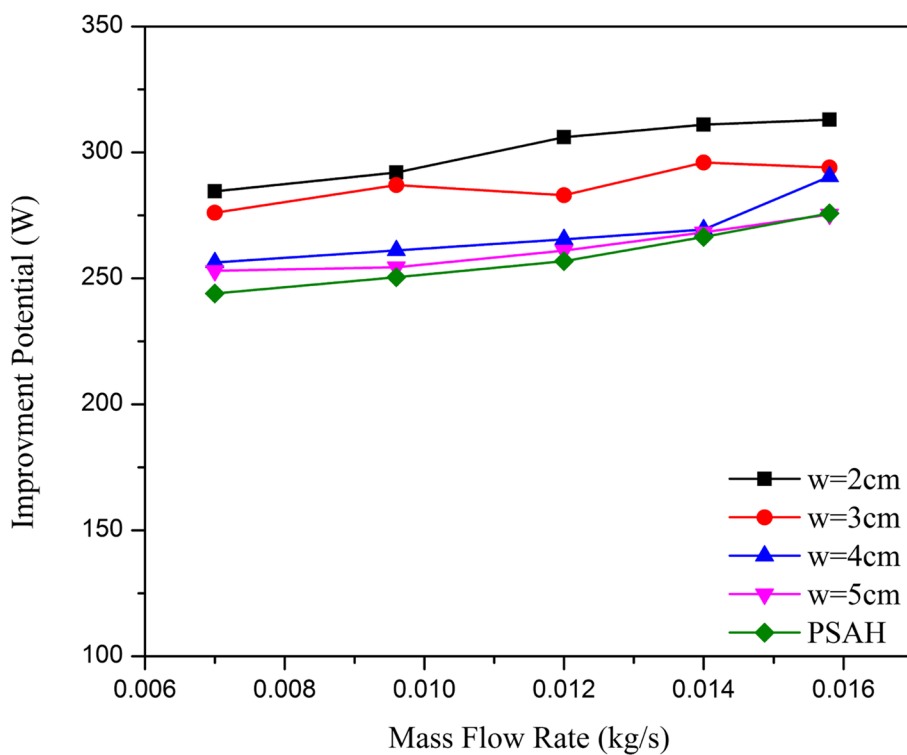**Fig. 11** MFR versus exergy destruction for various louvered fin spacings

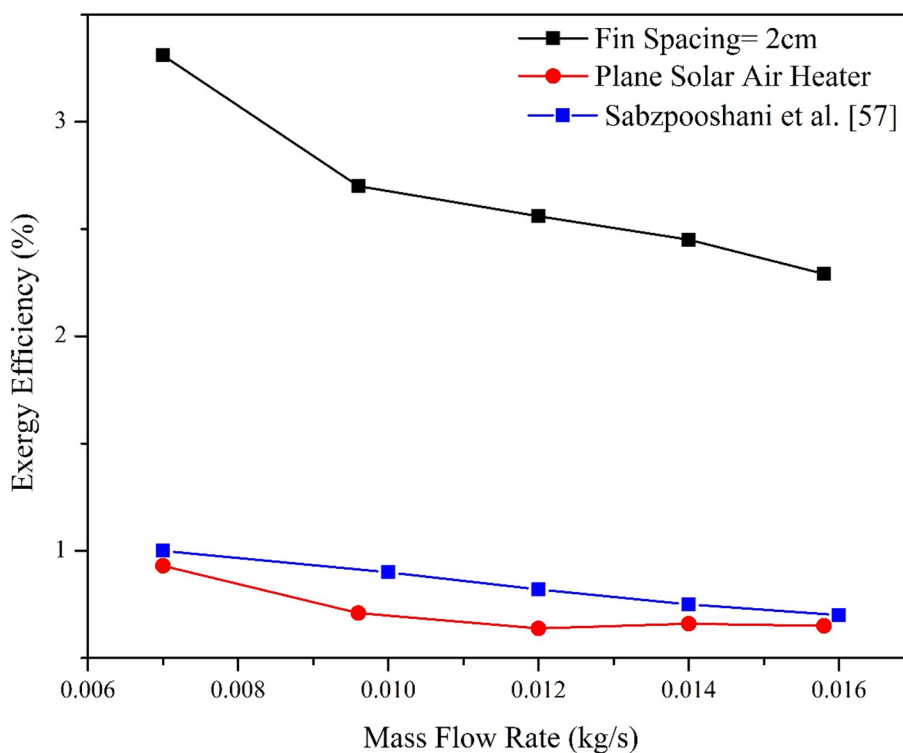**Fig. 12** Effect on improvement potential at various MFR for different fin spacing

Fig. 13 Comparison between the exergy efficiency of this study and that of Sabzpooshani et al. [58]

Table 4 Comparison of current work with preceding works

S. No	Collectors types	MFR and other parameters	Exergy efficiency	Reference
1.	Double-pass solar collector with fins	0.01–0.15 kg/s $I = 1000 \text{ W/m}^2$	Exergy efficiency, 2.5 to 4.2%	Assadeg et al. [59]
2.	Double-pass porous serpentine wire mesh packed bed SAH	0.01–0.05 kg/s	Exergy efficiency, 5.06 to $-$ 1.01%	Singh.S [60]
3.	Baffled solar air heater	0.004 to 0.04 kg/s	Exergy efficiency, 2 to 1.8%	Sabzpooshani et al. [58]
4.	LFSAH	0.0070–0.0158 kg/s	Exergy efficiency, 3.31%, 2.4%	Present work

The current study is contrasted with prior research in Table 4. The experimental results from both the present investigation and the earlier study indicate that the LFSAH demonstrates superior performance.

The exergy analysis results for LFSAH, acquired in Jamshedpur, Jharkhand, during the months of January and February 2018, are displayed in Table 5. From Eq. (11) to Eq. (13), exergy inlet and exergy outlet were calculated. In addition to this, the exergy optical losses, exergy destruction and second law efficiency and improvement potential (IP) were calculated from Eq. (14), Eq. (19), Eq. (20), and Eq. (21), respectively. Exergy losses were computed across different fin spacings and Flow Rates. It is crucial to emphasize that the maximum exergy loss occurred with a fin spacing of 5 cm at a flow rate of 0.0158 kg/s, whereas the minimum exergy loss was noted with a fin spacing of 2 cm at a flow rate of 0.007 kg/s. Furthermore, the exergetic performance of each fin spacing was

Table 5 Exergy analysis of louvered fin SAH

Fin spacing	Air flow rate (kg/s)	Exergy input (kW)	Exergy output (kW)	Exergy destruction (kW)	Optical losses (kW)	Improvement potential (kW)	Second law efficiency (%)
2 cm	0.007	0.17228–0.35137	0.00303–0.01165	0.15373–0.30809	0.01550–0.03162	0.15102– 0.29722	1.76–3.31
	0.0096	0.15421–0.34031	0.00207–0.0090	0.13826–0.30066	0.01389–0.03062	0.13640–0.29269	1.34–2.70
	0.012	0.16367–0.35665	0.00178–0.00937	0.14715 – 0.31518	0.01473–0.03209	0.14554–0.30689	1.09–2.66
	0.014	0.17984–0.38725	0.0026–0.01051	0.16139–0.34188	0.01618–0.03485	0.15936–0.33260	1.12–2.71
	0.0158	0.171.12–0.36052	0.00166–0.00823	0.15405–0.32053	0.01540–0.03222	0.15255–0.31382	0.97–2.29
3 cm	0.007	0.16230–0.36131	0.002717–0.01087	0.14497–0.31739	0.01460–0.03251	0.14255–0.30782	1.67–3.01
	0.0096	0.14453–0.33230	0.00145–0.00807	0.130.06–0.29432	0.01300–0.02990	0.12875–0.28716	1–2.4
	0.012	0.15115–0.32736	0.00127–0.00753	0.13627–0.29046	0.01360–0.02946	0.13513–0.28399	0.84–2.30
	0.014	0.14124–0.31876	0.00124–0.00609	0.12728–0.28404	0.01271–0.02868	0.12616–0.27866	0.88–1.95
	0.0158	0.12849–0.31878	0.00075–0.00564	0.11616–0.28444	0.01156–0.02869	0.11548–0.27938	0.590–1.78
4 cm	0.007	0.12859–0.29566	0.00104–0.00673	0.11597–0.26232	0.01157–0.02660	0.11502–0.25634	0.81–2.34
	0.0096	0.11234–0.31376	0.00089–0.00712	0.10133–0.27839	0.01011–0.02923	0.100528–0.27207	0.79–2.27
	0.012	0.12980–0.32384	0.00115–0.00789	0.11697–0.28679	0.01168–0.02914	0.11593–0.27988	0.88–2.3
	0.014	0.13231–0.30441	0.00093–0.00603	0.11946–0.27473	0.01190–0.02776	0.11862–0.26935	0.70–1.95
	0.0158	0.15363–0.33971	0.00113– 0.00678	0.13867–0.30234	0.01382–0.03057	0.13764–0.29630	0.74–1.99
5 cm	0.007	0.14577–0.31548	0.00162–0.00723	0.13102–0.28013	0.01311–0.02839	0.12956–0.27395	1.11–2.1
	0.0096	0.14980–0.32442	0.00139–0.00719	0.13493–0.28833	0.01348–0.02919	0.13367–0.28220	0.92–2.24
	0.012	0.16230–0.33705	0.00152–0.00648	0.14617–0.30022	0.01460–0.03033	0.14480–0.29444	0.93–1.94
	0.014	0.15086–0.31814	0.00103–0.00586	0.13625–0.27926	0.01357–0.02814	0.13531–0.27841	0.68–1.84
	0.0158	0.13221–0.30608	0.00100–0.00503	0.11931–0.27350	0.01189–0.02754	0.11840–0.26900	0.76–1.64

Chand *et al. Journal of Engineering and Applied Science*   (2024) 71:145

Page 19 of 22

assessed, revealing that the highest exergetic efficiency was attained with a fin spacing of 2 cm at a flow rate of 0.007 kg/s. Conversely, the minimum exergetic efficiency was noted for the fin spacing of 5 cm at a flow rate of 0.0158 kg/s.

Conclusions

This study entails conducting experimental investigations to evaluate the exergy efficiency of LFSAH under various operating conditions. The experimental assessments cover different MFR and fin spacings varying from 0.007 to 0.0158 kg/s and 2 to 5 cm, respectively.

The results have led to the following conclusions.

1. The experimental findings lead to the conclusion that the louvered fin spacing outperforms the PSAH.
2. The addition of louvered fins leads to a significant improvement in exergy efficiency when compared to PSAH for all MFR ranges.
3. The result revealed that the fin spacing of 5 cm in which the exergy loss is maximum for MFR of 0.0158 kg/s and the fin spacing 2 cm exergy loss is minimum at MFR of 0.007 kg/s.
4. The highest exergetic efficiency has been observed for the fin spacing 2 cm at 3.94% for MFR of 0.007 kg/s and the lowest exergetic efficiency has been found in fin spacing 5 cm at MFR of 0.0158 kg/s.
5. The exergy efficiency is improved by the attachment of louvered fins at the lower MFR, but as the MFR and fin spacing increased, the percentage of exergy efficiency decreases.
6. The exergy performance is enhanced by increasing the insolation, and the variations in exergy efficiency with MFR remain unchanged irrespective of the insolation.
7. In this study, various system and operating parameters have been addressed. However, there remain some aspects that could be explored in further studies. Investigating different geometries of louvered fins, such as corrugated or wavy louvered fins, could provide additional insights into enhancing heat transfer characteristics.

Abbreviations

A_c	Area of absorber plate, m^2
C_p	Specific heat (J/kgK)
DPFSAH	Double-pass finned solar air heater
DPVSAH	Double-pass V- shape finned solar air heater
Ex_i	Exergy input
Ex_o	Exergy output
Ex_{Lost}	Exergy lost
Ex_{Dest}	Exergy destruction
FSAH	Finned solar air heater
$\bar{h}$	Heat transfer coefficient
I	Insolation (W/m^2)
T_{fo}	Outlet temperature K
T_{fi}	Inlet temperature K
T_{fm}	Average fluid temperature
T_{pm}	Average plate temperature
LFSAH	Louvered fin solar air heater
$\dot{m}$	Mass flow rate (kg/s)
MFR	Mass flow rate
ΔP	Pressure drop

Chand *et al. Journal of Engineering and Applied Science*   (2024) 71:145

Page 20 of 22

PSAH   Plane solar air heater
Q_u Useful heat gain (W)
SAH   Solar air heater
PSAH   Plane solar air heater

Availability of data and materials
The data generated and/or analyzed during this study are available upon reasonable request from the corresponding author.

Declarations

Ethics approval and consent to participate
The participants had given their consent.

Competing interests
The authors declare that they have no competing interests.

References
1. Garg HP, Prakash J (2006) Solar energy fundamentals and applications. Tata McGraw Hill Publishing Co., Ltd, New Delhi
2. Khan BH (2006) Non-conventional energy resources. Tata McGraw Hill Publication, New Delhi
3. Ghritlahre HK. Performance evaluation of solar air heating systems using artificial neural network, Ph D Thesis
4. Ghritlahre HK, Sahu PK (2020) A comprehensive review on energy and exergy analysis of solar air heaters. Arch Thermodynam 41(3):183–222
5. Duffie JA, Beckman WA (2006) Solar engineering of thermal processes, 3rd edn. Wiley Interscience, New York
6. Choudhary C, Garg HP (1991) Design analysis of corrugated and flat plate solar air heaters. Renewable Energy 1(5/6):595–607
7. Mohammadi K, Sabzpooshani M (2013) Comprehensive performance evaluation and parametric studies of single pass solar air heater with fins and baffles attached over the absorber plate. Energy 57(1):741–750
8. Sahu MK, Sharma M, Matheswaran MM, Maitra K. On the use of longitudinal fins to enhance the performance in rectangular duct of solar air heaters—a review. J Sol Energy Eng 2019;141(3): https://doi.org/10.1115/1.4042827.
9. Chand S, Chand P, Ghritlahre HK (2022) Thermal performance enhancement of solar air heater using louvered fins collector. Sol Energy 1(239):10–24
10. Sharma SP, Saini JS, Varma HK (1991) Thermal performance of packed bed solar air heaters. Sol Energy 47:59–67
11. Varshney L, Saini JS (1998) Heat transfer and friction factor correlations for rectangular solar air heater duct packed with wire mesh screen matrices. Sol Energy 62(4):255–262
12. Mittal MK, Varshney L (2006) Optimal thermohydraulic performance of a wire mesh packed solar air heater. Sol Energy 80:1112–1120
13. Ghritlahre HK, Prasad RK (2018) Investigation of thermal performance of unidirectional flow porous bed solar air heater using MLP, GRNN, and RBF models of ANN technique. Therm Sci Eng Progress 6:226–235
14. Kumar A, Saini RP, Saini JS (2014) A review of thermohydraulic performance of artificially roughened solar air heaters. Renew Sustain Energy Rev 37:100–122
15. Behura AK, Prasad BN, Prasad L (2016) Heat transfer, friction factor and thermal performance of three sides artificially roughened solar air heaters. Sol Energy 130:46–59
16. Ghritlahre HK, Prasad RK (2018) Prediction of heat transfer of two different types of roughened solar air heater using artificial neural network technique. Therm Sci Eng Progr 8:145–153
17. Karsli S (2007) Performance analysis of new-design solar air collectors for drying applications. Renew Energy 32:1645–1660
18. Akpinar EK, Koçyiğit F (2010) Experimental investigation of thermal performance of solar air heater having different obstacles on absorber plates. Int Commun Heat Mass Transfer 37:416–21
19. Akpinar EK, Koçyiğit F (2010) Energy and exergy analysis of a new flat-plate solar air heater having different obstacles on absorber plates. Appl Energy 87(11):3438–3450
20. Alta D, Bilgili E, Ertekin C, Yaldiz O (2010) Experimental investigation of three different solar air heaters: energy and exergy analyses. Appl Energy 87(10):2953–2973
21. Ghritlahre HK (2021) An experimental study of solar air heater using arc shaped wire rib roughness based on energy and exergy analysis. Archives of Thermodynamics 42(3):115–139

22. Dincer I, Rosen MA. Exergy, energy, environment and sustainable development. 2nd Edition, Exergy Handbook. 2013 Elsevier, Oxford.
23. Mohtaram S, Chen W, Zargar T, Lin J (2017) Energy-exergy analysis of compressor pressure ratio effects on thermodynamic performance of ammonia water combined cycle. Energy Convers Manage 15(134):77–87
24. Mohtaram S, Chen W, Lin J. A study on an absorption refrigeration cycle by exergy analysis approach. In: IOP Conference Series: Earth and Environmental Science. 2018;182(1):012021. IOP Publishing.
25. Mohtaram S, Omidi M, Lin J, Sun H, Chen W (2019) Exergy analysis of a multi mixture working fluid absorption refrigeration cycle. Case Stud Therm Eng 1(15):100540
26. Chen L, Wang Y, Xie M, Ye K, Mohtaram S (2021) Energy and exergy analysis of two modified adiabatic compressed air energy storage (A-CAES) system for cogeneration of power and cooling on the base of volatile fluid. J Energy Storage 1(42):103009
27. Mohtaram S, Sun Y, Omidi M, Lin J (2021) Energy-exergy efficiencies analyses of a waste-to-power generation system combined with an ammonia-water dilution Rankine cycle. Case Stud Therm Eng 1(25):100909
28. Bani-Hani E, Assad ME, Alzara M, Yosri AM, Aryanfar Y, Castellanos HG, Mohtaram S, Bouabidi A (2023) Energy and exergy analyses of a regenerative Brayton cycle utilizing monochlorobiphenyl wastes as an alternative fuel. Energy 1(278):127861
29. Aryanfar Y, Mohtaram S, Alcaraz JL, Sun H (2023) Energy and exergy assessment and a competitive study of a two-stage ORC for recovering SFGC waste heat and LNG cold energy. Energy 1(264):126191
30. Kurtbas I, Durmus A (2004) Efficiency and exergy analysis of a new solar air heater. Renewable Energy 29:1489–1501
31. Kurtbase I, Turgut E (2006) Experimental investigation of solar air heater with free and fixed fins: efficiency and exergy loss. Int J Sci Technol 1(1):75–82
32. Chand S, Chand P (2018) Parametric study on the performance of solar air heater equipped with louvered fins. J Mech Sci Technol 32:3965–3973
33. Esen H (2008) Experimental energy and exergy analysis of a double-flow solar air heater having different obstacles on absorber plates. Build Environ 43:1046–1054
34. Gupta MK, Kaushik SC (2008) Exergetic performance evaluation and parametric studies of solar air heater. Energy 33(11):1691–1702
35. Gupta MK, Kaushik SC (2009) Performance evaluation of solar air heater for various artificial roughness geometries based on energy, effective and exergy efficiencies. Renewable Energy 34:465–476
36. Bouadila S, Kooli S, Lazaar M, Skouri S, Farhat A (2013) Performance of a new solar air heater with packed-bed latent storage energy for nocturnal use. Appl Energy 110:267–275
37. Benli H (2013) Experimentally derived efficiency and exergy analysis of a new solar air heater having different surface shapes. Renewable Energy 50:58–67
38. Bayrak F, Oztop HF, Hepbasli A (2013) Energy and exergy analyses of porous baffles inserted solar air heaters for building applications. Energy and Buildings 57:338–345
39. Velmurugana P, Kalaivanan R (2015) Energy and exergy analysis of multi-pass flat plate solar air heater—an analytical approach. Int J Green Energy 12:810–820
40. Acır A, Ata I, Şahin I (2016) Energy and exergy analyses of a new solar air heater with circular-type turbulators having different relief angles. Int J Exergy 20(1):85–104. https://doi.org/10.1504/IJEX.2016.076680
41. Ghritlahre HK, Prasad RK (2017) Energetic and exergetic performance prediction of roughened solar air heater using artificial neural network. Ciencia e Tecnica Vitivinicola 32(11):2–24
42. Abuşka M (2018) Energy and exergy analysis of solar air heater having new design absorber plate with conical surface. Appl Therm Eng 131:115–124
43. Matheswaran MM, Arjunan TV, Somasundaram D (2018) Analytical investigation of solar air heater with jet impingement using energy and exergy analysis. Sol Energy 161:25–37
44. Aktaş M, Şevik S, Dolgun EC, Demirci B. Drying of grape pomace with a double pass solar collector. Drying Technol. https://doi.org/10.1080/07373937.2018.1441154.
45. Aktaş M, Sözen A, Tuncer AD, Arslan E, Koşan M, Çürük O (2019) Energy-exergy analysis of a novel multi-pass solar air collector with perforated fins. Int J Renew Energy Dev 8(1):47–55
46. Kumar A, Layek A. Energetic and exergetic performance evaluation of solar air heater with twisted rib roughness on absorber plate. J Clean Prod 2019. https://doi.org/10.1016/j.jclepro.2019.05.363
47. Kumar A, Layek A (2021) Energetic and exergetic based performance evaluation of solar air heater having winglet type roughness on absorber surface. Sol Energy Mater Sol Cells 230:111147
48. Kumar D, Mahanta P, Kalita P (2021) Performance analysis of a solar air heater modified with zig-zag shaped copper tubes using energy-exergy methodology. Sustain Energy Technol Assess 46:101222
49. Das M (2022) Comparison of the performance of fixed and two-axis movable solar air heaters with different methods. Energy Sourc Part A: Recovery Utilization Environ Effects 44(1):195–217. https://doi.org/10.1080/15567036.2022.2028038
50. Prakash O, Kumar A, Dey K, Aman A (2022) Exergy and energy analysis of sensible heat storage based double pass hybrid solar air heater. Sustain Energy Technol Assess 49:101714
51. Khanlari A, Tuncer AD, Sözen A, Aytaç İ, Çiftçi E, Variyenli Hİ (2022) Energy and exergy analysis of a vertical solar air heater with nano-enhanced absorber coating and perforated baffles. Renewable Energy 187:586–602
52. Kline SJ, McClintock FA (1953) Describe uncertainties in single sample experiments. Mech Eng 7:3–8
53. Ghritlahre HK, Prasad RK (2018) Exergetic performance prediction of a roughened solar air heater using artificial neural network. Strojniški Vestnik – J Mech Eng 64(3):195–206
54. Ghritlahre HK, Prasad RK (2018) Exergetic performance prediction of solar air heater using MLP, GRNN and RBF models of artificial neural network technique. J Environ Manage 223:566–575
55. Ghritlahre HK, Prasad RK (2018) Prediction of exergetic efficiency of artificial arc shape roughened solar air heater using ANN model. Int J Heat Technol 36(3):1107–1115
56. Petela R (2008) An approach to the exergy analysis of photosynthesis. Sol Energy 82(4):311–328

57. Van Gool W. Energy policy: fairy tales and factualities. Innovation and Technology — Strategies and Policies. Soares A et al. eds. Springer, Dordrecht. 1997; p. 93–105. https://doi.org/10.1007/978-0-585-29606-7_6.

58. Sabzpooshani M, Mohammadi K, Khorasanizadeh H (2014) Exergetic performance evaluation of a single pass baffled solar air heater. Energy 1(64):697–706

59. Assadeg J, Al-Waeli AH, Fudholi A, Sopian K (2021) Energetic and exergetic analysis of a new double pass solar air collector with fins and phase change material. Sol Energy 15(226):260–271

60. Singh S (2020) Experimental and numerical investigations of a single and double pass porous serpentine wavy wiremesh packed bed solar air heater. Renewable Energy 1(145):1361–1387

Publisher's Note